Equatorial spread *F* initiation and growth from satellite traces as revealed from conjugate point observations in Brazil

M. A. Abdu,[1] E. A. Kherani,[1] I. S. Batista,[1] B. W. Reinisch,[2] and J. H. A. Sobral[1]

[1]   A better understanding of the precursor conditions for the instability growth is very important for identifying the causes of day-to-day variability in the equatorial spread *F* (ESF)/ plasma bubble irregularity development. We investigate here the satellite trace (S-trace) in the ionograms, a precursor to the postsunset ESF occurrence, as observed by Digisondes operated at an equatorial and two magnetic conjugate sites in Brazil during a 66 day observational campaign (Conjugate Point Equatorial Experiment 2002). The satellite traces first occur at the equatorial site, and sequentially, after a variable delay of approximately 20 to 50 min, they are observed nearly simultaneously over the two conjugate sites. The evening prereversal enhancement in the zonal electric field/vertical drift is found to control its development. Using a three-dimensional simulation code based on collisional interchange instability mechanism, it is shown that the observed S-trace occurrence sequence is fully consistent with the instability initiation over the equator with the field-aligned plasma depletion vertical growth marked by latitudinal expansion of its extremities to conjugate locations. The delay in the S-trace occurrence at the conjugate sites (a measure of the nonlinear growth of the instability for plasma depletion) is controlled also by field line parallel (meridional) neutral wind. The relationship between the S-trace and the large-scale wave structure in the *F* layer, another widely known characterization of the precursor condition for the ESF development, is also clarified.

1. Introduction

[2] Equatorial spread *F* (ESF)/plasma bubble irregularity development from precursor conditions of the background ionosphere and thermosphere is a subject of great current interest. The irregularities develop from plasma instability processes that set in at the nightside of the sunset terminator, when the basic prerequisites for instability growth are present. In a typical case, the instability grows from Rayleigh-Taylor interchange instability mechanism initiated by density perturbations with polarization electric field operating at the bottomside density gradient region of a rapidly rising *F* layer. The most important prerequisites for the instability growth can be specified as follows: (1) the postsunset rise of the *F* layer due to the prereversal enhancement in the zonal electric field (PRE)/vertical plasma drift arising from sunset electrodynamics of the *F* layer dynamo, (2) wave modulation of the *F* layer bottomside, in the form of altitude modulations, commonly attributed to gravity waves (GWs) that provide the seed

perturbations in polarization electric field and density, which are required to initiate the instability growth, and (3) the upward density gradient of the *F* layer bottomside. The large degree of the day-to-day variability, widely observed in the ESF occurrence, arise from the variabilities in these driving parameters. Item (3) will not be of our specific concern here, since its variability must in some way be related to the other two drivers. The PRE that has been more widely investigated is found to be the most direct driver of ESF development in statistical as well as event-based studies, especially for the vertical drifts/layer base height larger than a threshold value [*Abdu et al.*, 1983, 2009a, 2009b; *Fejer et al.*, 1999; *Chapagain et al.*, 2009]. Such threshold can vary from one day to the other as a result of the variability in the degree of wave modulation, that is, the seed perturbation amplitude needed for initiating the instability growth. In the literature there are varying characterizations of the nature of the seed perturbation. The most basic source of the seed perturbation is known to be the gravity waves that must be present in the evening thermosphere. From observations by different techniques and from theoretical and model studies it is now well recognized that the gravity waves originating from sources of their generation in tropospheric convective regions do propagate to thermospheric heights [*Röttger*, 1973; *McClure et al.*, 1998; *Fritts et al.*, 2008; *Liu and Vadas*, 2013]. In statistical terms the ESF seasonal/monthly occurrence characteristics have been correlated with the tropospheric convective activity

---

[1]Instituto Nacional de Pesquisas Espaciais, São Jose dos Campos, Brazil.
[2]Lowell Digisonde International, LLC, Lowell, Massachusetts, USA.

Corresponding author: M. A. Abdu, Instituto Nacional de Pesquisas Espaciais, Ave. dos Astronautas, 1758 Jd da Granja, São Jose dos Campos, São Paulo 12242-970, Brazil. (maabdu@dae.inpe.br)
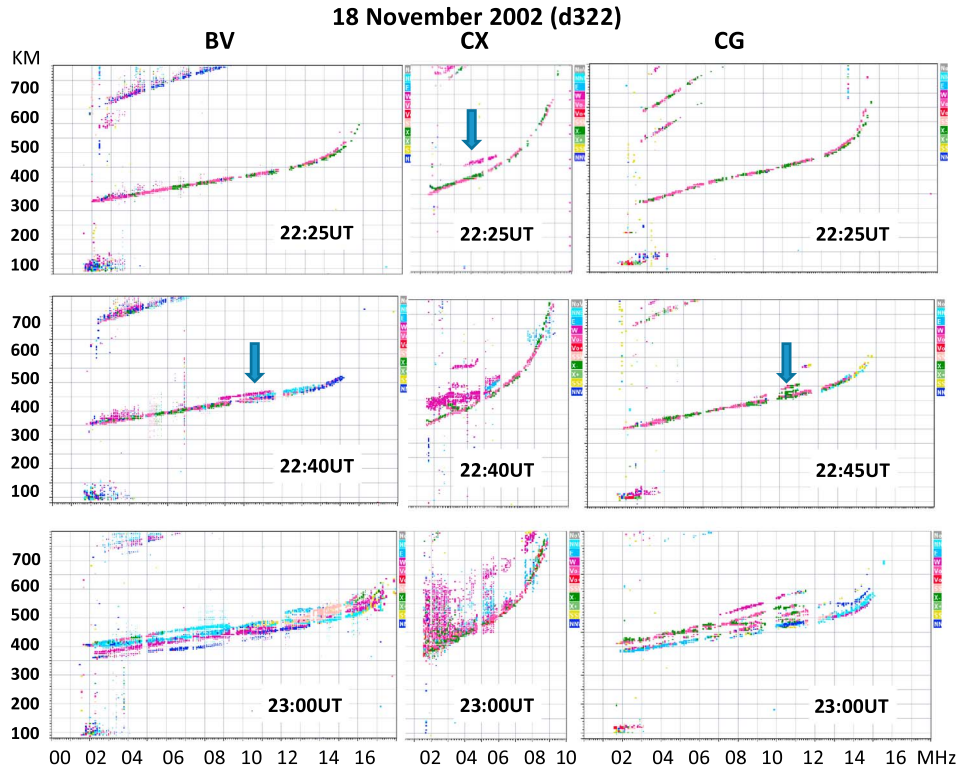
18 November 2002 (d322)

Figure 1. Ionograms from the equatorial site Cachimbo (CX) and the conjugate sites, Boa Vista (BV) and Campo Grande (CG), showing the start of the S-trace (indicated by a down-looking arrow), first at 22:25 UT over CX and later at 22:40 UT and 22:45 UT, respectively, over the two conjugate sites.

as represented by the Intertropical Convergence Zone, as well as by the outgoing longwave radiation [*Tsunoda*, 2010]. Based on case studies, it was shown by *Abdu et al.* [2009a] and *Kherani et al.* [2009] that gravity wave contribution as a precursor seed to ESF instability growth was well observable by a Digisonde [*Reinisch*, 1996; *Reinisch et al.*, 2009] when the PRE vertical drift was smaller than a statistical threshold value, whereas for larger PRE amplitudes the gravity wave contribution was barely observable. Another way of characterizing the precursor wave modulation is through the quasi-periodic large-scale wave structure (LSWS) originally described as such by *Tsunoda and White* [1981] who found that the LSWS having east-west scale dimension of the order of 400 km was a necessary precursor for ESF growth in the few cases that they studied using the Altair radar east-west scan measurements. More recently, observations of LSWS in total electron content (TEC), also of similar scale sizes (300–800 km), as obtained from radio beacon observations on board Communications/Navigation Outage Forecasting System (C/NOFS) satellite were reported by *Thampi et al.* [2009], *Tsunoda et al.* [2011], and *Tulasi Ram et al.* [2012]. The LSWS began well before the *E* layer sunset and continued into postsunset ESF development, very similar to the gravity wave oscillations in *F* layer height starting at presunset hours that lead to the postsunset ESF growth [*Abdu et al.*, 2009b]. Yet another ESF precursor signature, as seen in ionosonde data, concerns the satellite traces that appear adjacent to the *F* layer trace [e.g., *Abdu et al.*, 1981; *Lyon et al.*, 1961]. With some rare exception the satellite traces preceded all the ESF occurrences over Fortaleza in the study by *Abdu et al.* [1981]. From simultaneous ionosonde and incoherent scatter radar observations over Kwajalein Atoll, *Tsunoda* [2008] identified the satellite traces as causally associated with the occurrence of LSWS. A recent study by *Li et al.* [2012] based on VHF backscatter radar and Digisonde observations at a low-latitude site, Sanya (China), showed that the LSWS-ESF connection is operative when the PRE has nonnegligible amplitude, meaning that the LSWS does not lead to ESF development when the PRE amplitude is inexpressive. In the present work we investigate the connection between the satellite trace, the LSWS, and postsunset ESF through observations of the satellite trace developments concurrently at an equatorial and two low-latitude conjugate sites during a 2 month long observational campaign conducted in Brazil (the Conjugate Point Equatorial Experiment (COPEX) campaign) [*Abdu et al.*, 2009a; *Batista et al.*, 2008; *Reinisch et al.*, 2004]. By comparing the observational data with results of a 3-D instability simulation, we present a quantitative evaluation of the connection between the satellite trace appearance and the ensuing bubble development as observed at the equatorial and conjugate sites. It is further shown that the satellite traces (hereafter denoted as S-trace) developing at a specific phase of the PRE represent the early phase of a growing instability whose nonlinear growth to form topside depletions is controlled by the PRE amplitude as well as by transequatorial wind.

2. Data Analysis and Results

[3] Three Digisondes were operated during a 66 day period (October–December) of the COPEX (Conjugate Point Equatorial Experiment) campaign conducted in Brazil in 2002. The three stations were located such that the conjugate
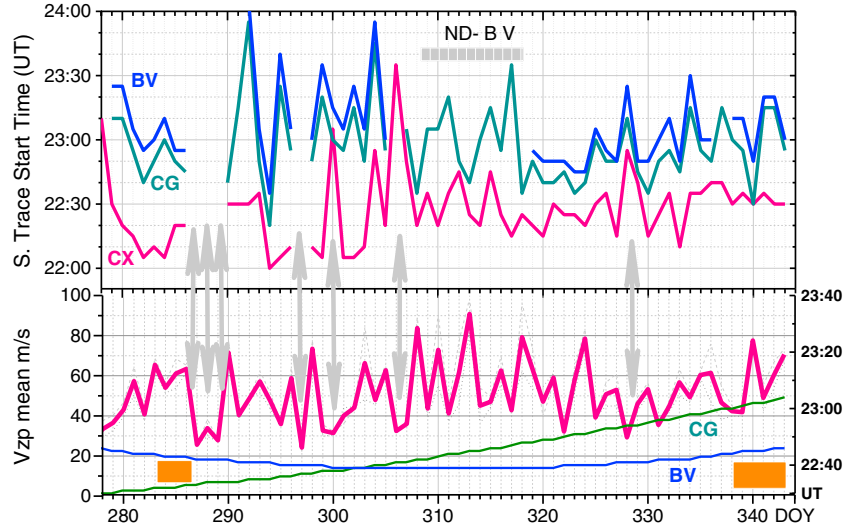
Figure 2. (top) The start times of the S-trace occurring first over CX (pink) and later over the conjugate sites (blue and green) during a period of 66 days (from October to December 2002). Please note that the S-trace start times over BV (blue curve) have been displaced upward by 10 min for easier identification when they are the same as those over CG. (bottom) The variation in the prereversal vertical drift velocity peaks (pink) during the period. The conjugate point *E* layer (100 km) sunset times are shown by blue and green lines over BV and CG, respectively (right axis). The orange bars indicate the intervals that formed the Q1 and Q2 days discussed in the text. ND, no data.

E layers were field line mapped to the *F* layer bottomside over the magnetic equator. The stations are the following: Campo Grande (CG): 20.43°S; 54.63°W; dip: −22.3° (southern conjugate point); Boa Vista (BV): 02.81°N, 60.66°W; dip: 22° (northern conjugate point); and Cachimbo (CX): 9.46° S, 54.83°W; dip: −4.25° (near dip equator). (A map of these stations can be found in *Abdu et al.* [2009a].) Exactly identical antenna systems for transmission and reception were used at all three sites, and the data analyzed in this paper were collected at a 5 min cadence. The satellite traces that occur adjacent to the first hop *F* layer trace are analyzed here. The times of their first appearance (onset time) at all the stations on all the campaign days were carefully identified. These times are analyzed as a function of the evening prereversal vertical drift amplitude of the individual days as well as the conjugate *E* layer sunset times.

2.1. Characteristics of the Conjugate Point S-Traces

[4] Figure 1 shows an example of a sequential occurrence of the S-traces at the COPEX sites on 18 November 2002. The S-trace first appeared close to the *F* layer trace over Cachimbo (CX) at 22:25 UT/18:45 LT (LT = UT − 3 h 40 min), indicated by a down-pointing arrow. At this time no S-trace was present at either of the conjugate sites. The S-trace over the conjugate sites first appeared with a time delay, and nearly simultaneously (that is, within a time difference of less than the 5 min observation cadence), as can be noted in the ionograms at 22:40 UT/19:00 LT over Boa Vista (BV) and 22:45 UT/19:05 LT over Campo Grande (CG). The time delay in this case was 15–20 min, by which time the spread *F* over Cachimbo was further developed (as can be seen in Figure 1 (middle)). What this sequence tells us is that the S-trace over Cachimbo must have originated from the bottom edge of a developing plasma depletion/bubble whose flux-tube-aligned vertical growth (by the

Rayleigh-Taylor instability mechanism) to an apex height of around 650 km (over the dip equator) was responsible for its extremities to extend in latitude to the conjugate point *F* layers, where the S-traces subsequently occurred nearly simultaneously. The elapsed time being ~15–20 min, the vertical rise velocity of the depletion was close to 200 m/s, in this case. With the bubble vertical growth, the bottomside spread *F* (SF) intensified over Cachimbo as seen in the ionogram at 22:40 UT. By 23:00 UT the SF over CX is close to being fully developed, when the conjugate sites show more evolved and multiple S-traces that subsequently evolved into the standard spread *F* diffuse traces in the next ionograms (not shown here). It is interesting to note that the frequency at which the S-trace first appeared over CX (Figure 1) was near 4 MHz, whereas this frequency was near 10–11 MHz over BV and CG. The higher frequency of the S-trace over the conjugate sites as compared to its lower frequency over the equatorial site is a common feature (with some exceptions) in our data. There appear to be two reasons for this: (1) The *F* layer over the conjugate sites, being closer to the equatorial anomaly ionization crest, is clearly denser than that in the ionization trough over the dip equator, as can be verified by noting that the f_oF_2 over BV and CG is near 15 MHz whereas its value over CX is only around 9 MHz (in Figure 1). This leads to a situation where the electron density modulation responsible for the S-trace echoes over the conjugate sites operates on a higher background ionization (and therefore higher plasma frequency to be reflected) as compared to that over the equator. (2) The magnetic flux tube-aligned plasma depletion developing upward over the equator that attains a high-enough apex height with sufficient depletion intensity should specify the height region (and therefore the plasma frequencies) over low-latitude conjugate sites that can produce S-traces over these sites. A more quantitative evaluation of these effects is beyond the scope of this study.
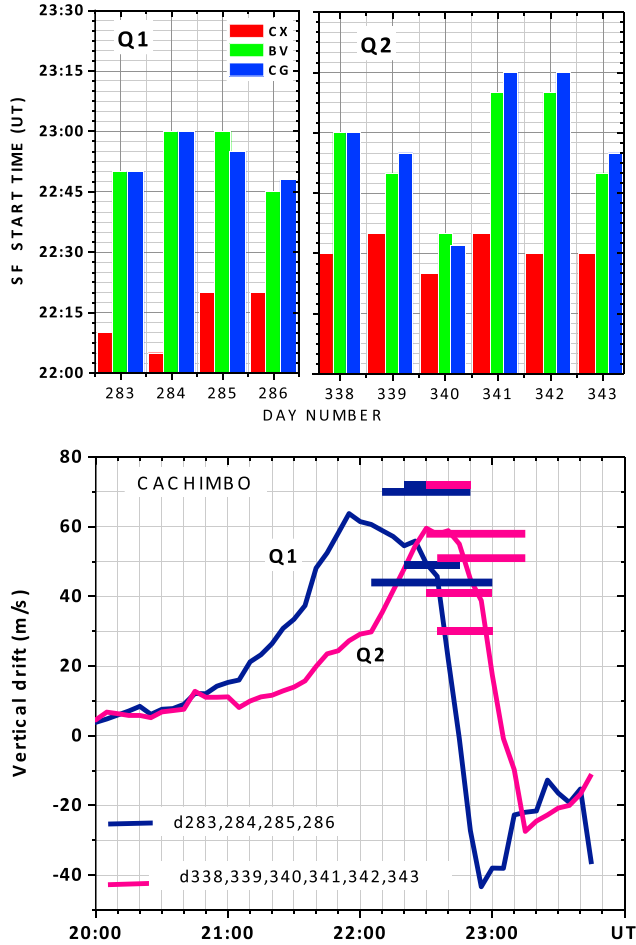
Figure 3. (top) The S-trace onset times, at CX, BV, and CG, during two groups of days (Q1 and Q2) representing an earlier and a later part of the entire period (of Figure 2). (bottom) Averages of the vertical drifts for the Q1 and Q2 days over Cachimbo. The horizontal bars indicate the S-trace start time at CX connected to that at the conjugate sites for the individual days of the two groups of days, color coded to correspond to their respective mean vertical drift. The bars are plotted at the vertical drift values at the start of each S-trace over CX.

[5] The S-trace occurrence sequences over the three sites for the entire campaign period of 66 days are presented in Figure 2, wherein Figure 2 (top) shows the S-trace onset times in UT over Cachimbo (CX) (in pink), Campo Grande (CG) (in green), and Boa Vista (BV) (in blue). A period of no data (ND) over BV is marked from day 308 to day 318. We note that the S-trace first appears always over Cachimbo (in general after 22 UT) with significant day-to-day variation in its occurrence time. Over the conjugate sites the S-traces appear with a delay of a few tens of minutes varying from one day to the other. It is important to note that irrespective of the onset time at CX and the delay time from it, the S-trace occurrences over the conjugate sites are nearly "simultaneous", being always within the 5 min observation cadence. (Please note that the S-trace start times over BV are displaced upward by 10 min for easy identification when these values are the same as those over CG). This important characteristic was already apparent in Figure 1, which thus supports the scenario of their connection through the vertical growth over the dip

equator of field-aligned plasma depletion instability, whose observed early phase was the first sighting of the S-trace over the equatorial site. All cases of the S-trace occurrence were followed by spread *F* (SF) development at the respective sites (except on day 306 which appeared to be a doubtful case of an S-trace).

[6] Figure 2 (bottom) shows the PRE peak vertical drift amplitude (V_{zp}) over Cachimbo and the sunset (SS) local times at the conjugate *E* layers (at 100 km). The vertical drift was deduced as the time rate of change of the *F* layer true heights, d(hF)/dt, [*Abdu et al.*, 2006], and the plotted values are averages of the drifts at a few plasma frequencies (5, 6, 7, and 8 MHz). A comparison of the results in the two panels brings out the following important observational points: (1) the PRE vertical drift amplitude appears to have significant control over the SF development (as has also been found previously from statistical analysis of ionosonde and radar data) [*Abdu et al.*, 1983, 2009a; *Fejer et al.*, 1999]. Some clear examples can be noted on days 287, 288, 289, 297, 300, 328, and 306, when the large dips in the vertical drift, indicated by the vertical arrows, correspond to nonoccurrence, or delayed occurrence, of the S-trace and SF, at the equatorial and/or the conjugate stations; (2) the delay in the S-trace onset at conjugate sites with respect to that at the equatorial site, which is a measure of the bubble vertical growth rate, appears to be a bit longer during the first half of the observational period as compared to the latter half when the delay is statistically smaller. Correspondingly, we may infer that the bubble growth was generally slower during the former interval with a more rapid growth in the latter interval (this will be discussed later using model results); and (3) the onset time of the S-trace over the equator appears to follow roughly the later of the conjugate point sunset times. We may especially note a trend of a slow increase in the S-trace start time over Cachimbo (forward of the day around 300) with the increase in the SS time when it occurs later over CG. The characteristics in the items (2) and (3) are a result of the modulation of the background drivers that vary with the seasonal transition of the ionosphere from equinox to summer in the Brazilian region.

[7] Some additional highlights of the above results are presented in Figure 3, in which we compare the results between two groups of days, Q1 days (283, 284, 285, and 286) and Q2 days (338, 339, 340,341,342, and 343), selected, respectively, from an earlier and a later part of the campaign interval as denoted by orange bars in Figure 2 (bottom). The two groups of days were selected because they represent slightly displaced phases of the seasonal transition (from equinox to southern summer) that marked the COPEX campaign period as can be noted from the *E* layer sunset times at the conjugate sites (in Figure 2) that progressively moved to later hours during the period. We notice, in Figure 3 (top), that the S-trace start time over CX is generally earlier on the Q1 days than on the Q2 days. Further, the delay in the S-trace occurrence over the conjugate sites with respect to CX is generally more in the former than in the latter case. However, as pointed out before, the S-trace onset is nearly simultaneous at the conjugate sites in all the cases. The *F* layer vertical drift velocity during its evening prereversal enhancement period over Cachimbo is shown in Figure 3 (bottom) as separate averages for the Q1 and Q2 day groups. The PRE vertical drift velocity, V_{zp}, peaks at about 60 m/s for the two groups of days.

Also shown in the figure are horizontal bars connecting the times of the first appearance of the S-trace over the equator to those over the conjugate sites (thus indicating the conjugate point delay time of the S-Trace (DTST)) for individual days in the two groups. The end time of the bars corresponds to the average time of the S-trace onsets at the two conjugate sites. (The horizontal bars have the same color coding as that of their corresponding mean Q1 and Q2 vertical drift curves, and they are positioned at the vertical drift values at the start of each S-trace.) We may note that (1) the evening drift enhancement (PRE) starts to develop earlier on the Q1 days than on the Q2 days so that the local time of the corresponding V_{zp} occurs around 40 min earlier on the former than on the latter days. This time delay could be the result of the seasonal transition, from equinox to summer, in the background ionosphere; (2) the S-trace begins generally near or after the vertical drift peak, and thus, its appearance is displaced in local time corresponding to the relative displacement in the PRE development between the two groups of days. It thus appears evident from these results that the S-trace development in these cases is controlled by the PRE development. The local time displacements in the S-trace bars, with respect to the PRE peak, however, appear to be relatively less on Q2 days than on Q1 days. (The significance of the connection between the S-trace, the LSWS, and the PRE for ESF initiation will be discussed below.)

3. Discussion

[8] The satellite trace sequence characterized by its near-simultaneous appearance over conjugate sites, which is delayed by a few tens of minutes from its first appearance over the dip equator, appears to be a manifestation of the plasma bubble instability growth process as we now understand it. The field-aligned depletion initiated over the equator by the Rayleigh-Taylor interchange instability mechanism develops upward extending also in latitude. The S-trace over Cachimbo represents the ionogram signature of the bottom edge of the depletion over the equator, and those over the conjugate sites (CG and BV) represent the low-latitude ends of the field-aligned depletion that attained an apex altitude of around 650 km over the equator. In this way, the time the depletion takes to attain the apex altitude from its initiation at the equatorial F layer bottomside is responsible for the DTST. It may be noted that for similar PRE vertical drifts during the earlier and later parts of the observational interval the DTST tends to be larger (generally) in the former case than in the latter case, as can be verified by comparing, for example, the days before day 305 with the days after day 318 (in Figure 2). This means that the nonlinear vertical growth of the depletion is slower in the former case (including the Q1 days) than in the latter case (that include the Q2 days). This behavior can be related to the fact that the transequatorial/meridional wind in the evening hours that was more southward during October decreased in intensity, tending to reverse to northward in December [see also *Abdu et al.*, 2009a]. This marked the seasonal transition that characterized the campaign period.

[9] Using a three-dimensional simulation model based on the collisional interchange instability (CII) mechanism [*Kherani et al.*, 2005], we have verified the connection between the S-trace over the equatorial site with that over the conjugate sites (manifested by the DTST). The plasma bubble simulation was performed in the altitude-longitude-latitude frame and used the background ionosphere conditions (such as the evening vertical drift and the bottomside electron density profile) as those observed during the Q1 and Q2 days. The model was run for the following conditions: Case I: ionospheric conditions corresponding to the Q1 days; Case II: Case I + a magnetic field-aligned wind of 80 m/s; and Case III: ionospheric conditions corresponding to the Q2 days. The seeding perturbation in the form of a gravity wave of amplitude = 5 m/s and horizontal east-west wavelength = 300 km was chosen for all the three cases. The corresponding amplitude of the density perturbation was ~5%. The simulation begins at T_i = 21:10 UT and 21:40 UT for Q1 and Q2, respectively. These initial times for the Q1 and Q2 cases are chosen because at these hours the Vz becomes equal to 20 m/s for both Q1 and Q2, as can be noted from Figure 3. The 20 m/s is the average vertical drift of the daytime ionosphere, and the prereversal drift enhancement (that exceeds the average daytime drift) usually begins after the drift attains this value. Therefore, choosing 20 m/s as a starting time for both Q1 and Q2 ensures that the ambient conditions (such as the longitudinal gradient in the E region conductivity and the ratio of the E to F region Pederson conductivity) that are responsible for the prereversal drift are similar in both the cases. The simulation results are presented in Figure 4 depicting the altitude-latitude-temporal evolution of the degree of depletion $\Delta n / n_{max}$ = 30%. Here the $\Delta n = n - n_{max}$ where the n_{max} is the density inside the blob or enhancement located adjacent to the depletion. For any given time, both n and n_{max} are estimated for each latitude and altitude so that the effects of the spatial variation of the ambient density in the estimation of the $\Delta n/n_{max}$ are removed. The $\Delta n / n_{max}$ = 30% level is chosen because it corresponds to an intermediate state between the seeding amplitude and a developed plasma bubble and can be regarded as a cursor for the satellite trace. The latitude and time are drawn as axes while the altitude is represented as the contours with pixmap colors as described by a color bar. Figure 4d depicts the latitude-temporal evolution of $\Delta n / n_{max}$ = 30% at 375 km altitude for Cases I–III and is obtained by picking the 375 km contour from the results of Figures 4a–4c. The red, green, and blue contours correspond to Cases I, II, and III, respectively. It may be noted that the 30% depletion produces closed contours, thereby showing that at any given latitude the depletion occurs twice in the course of the simulation (see, for example, at the 11.1° vertical line in Figure 4). The first occurrence (at the earlier time) is during the upward phase of the PRE vertical drift whose reversal to downward can be noted near 22:45 UT and 23:05 UT for the Q1 and Q2 cases, respectively, in Figure 3. The second time occurrence of the depletion is caused by the downward phase of the PRE vertical drift. A dashed red line for Case I, a dashed green line for Case II, and a dashed blue line for Case III are drawn to indicate the time interval, ΔT, between the time of appearance of the 30% depletion level at 375 km over the equator and the appearance of the same depletion level over 11° latitude (close to the conjugate sites). Here ΔT represents the time interval of the mapping and can be considered as equivalent to the DTST.

[10] We may note from Figures 4a–4c that the 30% depletion at any height first develops over the equator and then with the time delay, ΔT, maps to the off-equatorial latitudes. It may be noted that right at the equator as the time increases, the 30% depletion moves to higher altitudes, that is, the
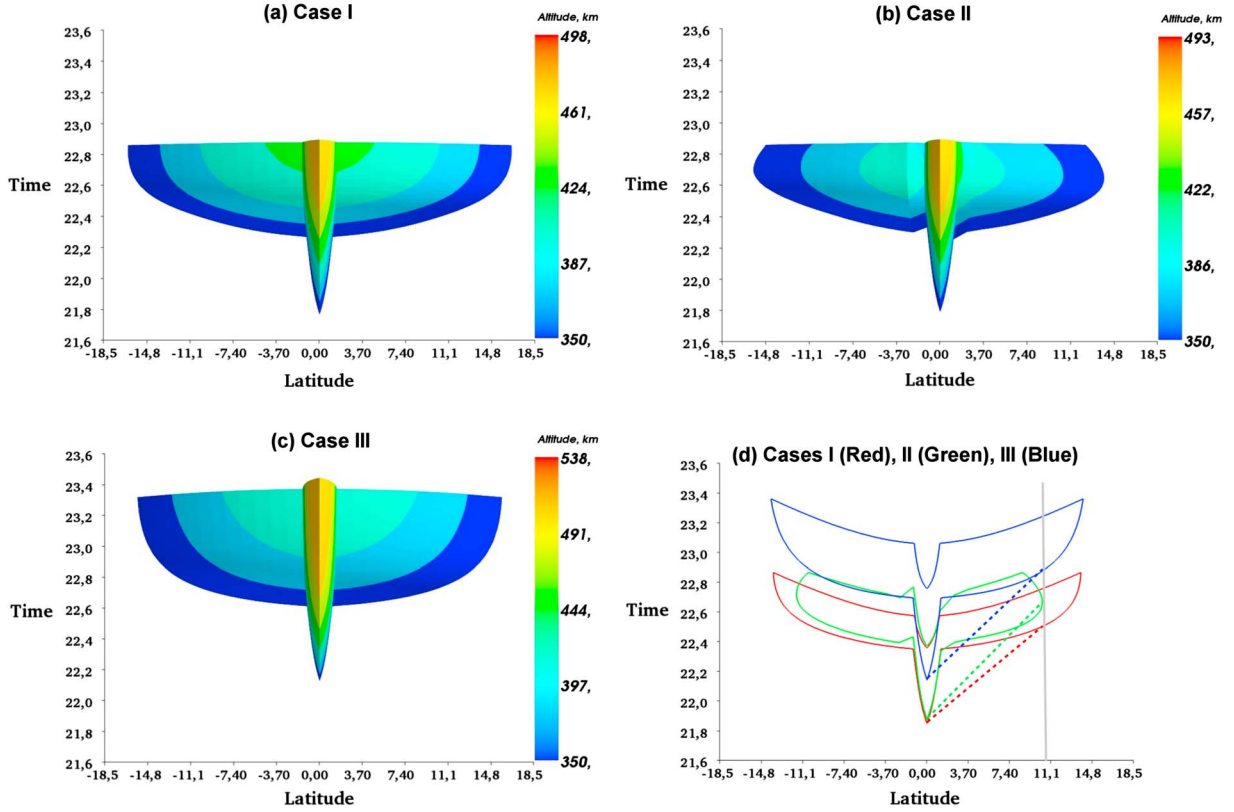
Figure 4. Model simulation results of 30% depletion excited by CII: (a–c) the latitude-altitude-temporal evolution of 30% depletion for the three cases described in the text. The latitude and time (in UT) are drawn as axes, and the altitudes are drawn as contours with pixmaps, as described by a color bar. (d) The latitude-temporal evolution of 30% depletion at altitude = 375 km, by picking an isoaltitude (= 375 km) contour from Figures 4a–4c, is plotted for Cases I (red contour), II (green contour), and III (blue contour). Cases I and II (that is, without and with 80 m/s field-aligned wind, respectively) represent the Q1 days, and Case III represent the Q2 days as described in the text. The dashed straight lines indicate the delay time corresponding to the DTST (see the text) that may be directly compared with the observed DTST as seen in the Figures 2 and 3.

depletion develops upward with time. It also extends to off-equatorial latitude with increase in time. However, at any given time the height versus latitude variation of the 30% depletion is not aligned with magnetic field line. In other words, although the plasma depletions are known to be field aligned, the degree of depletion in a field-aligned structure varies along a given field line. As a result, while the 30% depletion developed at lower apex altitude maps to the higher off-equator latitude that developed at higher apex altitude does not map that far. In addition, the degree of depletion is estimated for a fixed longitude inside a depletion. At fixed longitude, the degree of the depletion increases with altitude at the equatorial bottomside *F* region, leading to the confinement of the 30% depletion to the lower latitude as altitude increases. We also note that under Cases I and III, the mapping is symmetric across the equator. On the other hand, under Case II, which considers a magnetic field-aligned wind of 80 m/s, the mapping becomes asymmetric such that a contour is more extended toward southern latitudes which are the direction of meridional wind flow.

[11] From Figure 4d, we also note that the time interval of mapping, ΔT, is different for different cases. Under Case I, the 30% depletion at 375 km first develops over the equator at $T_o = 21:53$ UT (18:13 LT) and maps to the latitude = 11° (close

to the conjugate site latitude) at $T = 22:30$ UT (18:50 LT), i.e., $\Delta T = 37$ min. Thus, the simulation with Case I shows that the $\Delta T \approx 37$ min for Q1 days which is somewhat less than an average of the observed DTST ≈ 45 min. For Case II, which uses a field-aligned wind of 80 m/s, on the other hand, we note that $\Delta T \approx 22:39 – 21:53$ UT = ~ 46 min as determined from the dashed green line. Therefore, the Case II, which represents the Q1 days with the inclusion of a field-aligned wind (or meridional wind), provides larger DTST value that shows more delayed depletion growth that is consistent with the observations during Q1 days. As mentioned before, the inclusion of wind during Q1 days is justified because the meridional wind near sunset hours is larger during the Q1 days of October as compared to its nearly zero values during the Q2 days of December [see *Abdu et al.*, 2009a, Figure 8]. The simulation result does show that an increase (decrease) in the meridional/transequatorial wind could cause a decrease (increase) in the bubble nonlinear growth rate [see also *Maruyama*, 1988; *Abdu et al.*, 2009a].

[12] For Case III corresponding to the Q2 days, we may note that the 30% depletion at 375 km begins to develop over the equator at $T_o = 22:09$ UT (18:29 LT) and maps to the latitude of 11° at $T = 22:53$ UT (19:13 LT). Here the ΔT (DTST) ~ 44 min as determined from the dashed blue line.

The values of T_o and ΔT are reasonably compatible with the beginning time of the satellite trace at the equator and the observed DTST value during Q2 days (see Figure 2). It can thus be said that the evolution and mapping dynamics of the 30% level of depletion under Cases II and III consistently explain the observed satellite trace parameters during Q1 and Q2 days, respectively. This suggests that the S-traces constituting a precursor to the ESF are not just an altitude modulation of the F layer bottomside, but that they do represent the growth phase (of the order of 30% depletion level) of an ESF, as indicators of the instability growth.

3.1. On the LSWS-S-Trace-PRE Connection and ESF

[13] From a case study of simultaneous incoherent scatter radar and ionosonde data, *Tsunoda* [2008] showed that the S-trace in the ionograms is causally related to LSWS. Earlier, *Tsunoda and White* [1981] showed that the ESF/bubble irregularities developed from the upwelling or the crest of the LSWS. The present result showing a significant/strong influence of the PRE on the S-trace development (and hence on the ESF irregularity growth) therefore raises the question as to whether the LSWS should also be in some way controlled/influenced by the PRE. This question, however, is not a straightforward one to answer.

[14] In other words, the PRE control of the S-trace found in our result suggests the existence of a mechanism for such control, and it is interesting to speculate as to how that mechanism could defer from (or be similar to) a possible PRE influence on the LSWS development if it can be identified at all. To answer this we need to take a broader perspective. We note that a good correlation between the mesoscale structure in the electric field/vertical drift before sunset and locations of large plasma bubbles after sunset was shown by *Eccles* [2004] from an analysis of San Marco satellite data. The presunset wave structure was observed on magnetic field lines that have large field line-integrated F region conductivity compared to the E region during the late afternoon and evening, which suggested that atmospheric gravity waves in the F region were responsible for the wave structure/modulations in the vertical plasma drift. In this context we point out that (1) *Abdu et al.* [2009b] found the presence of gravity wave oscillations in equatorial F layer heights before sunset hours over Fortaleza that continue to postsunset hours and, in the presence of the PRE, contributed to topside bubbles as diagnosed by a VHF radar and a Digisonde. On all the days of the present study shown in Figure 2, gravity wave oscillations with varying intensity were present in the evening hours (not shown here) that lead to the postsunset spread F development. (2) Wave oscillations in the TEC, as diagnosed from radio beacon experiment on board the C/NOFS satellite, were observed before the E layer sunset by *Thampi et al.* [2009], *Tsunoda et al.* [2011], and *Tulasi Ram et al.* [2012]. These oscillations were identified as signatures of LSWS that grew in amplitude to the postsunset hours where instability processes lead to plasma depletions. These sets of different types of observations suggest that oscillations in vertical drift, layer height, and TEC, driven by a gravity wave-induced polarization electric field, must be a regular feature in the late afternoon/presunset equatorial ionosphere. They appear to be sustainable under the large field line-integrated F region conductivity compared to the E region conductivity that prevails at these hours. The PRE associated vertical drift and the

F layer uplift are responsible for further growth of these oscillations through the Rayleigh-Taylor (R-T) interchange instability process that results in the postsunset plasma depletion/bubble development. Our results suggest that the S-trace onset is an indicator of a plasma depletion growth phase marking the initiation of an ESF instability process. The LSWS amplitude as seen in the ΔTEC also increases toward postsunset hours due to the increasing contribution to ΔTEC from the growing plasma depletion.

[15] Here we may make an observation on the possible factors contributing to the ESF day-to-day variability. In Figure 3, a delay in the S-trace onset with respect to the growth of the PRE was observed, which, obviously, is a result of the time it takes for the instability to grow (growth time) once the required linear growth rate becomes significant enough for such growth. We know that the PRE contributes to the linear growth rate. An important criterion for the instability growth must, however, be the occurrence of a gravity wave-induced polarization electric field of sufficient intensity (eastward electric field perturbation) at a phase of the PRE growth that provides also plasma vertical drift of sufficient intensity. Since independent sources/mechanisms are believed to operate in the PRE development and in the GWs generation, the possibility of their phases occurring in a most favorable condition for instability growth may vary from one day to the other, thereby accounting for a significant component of the causes of the ESF day-to-day variability. Another aspect of the problem is related to the requirement of the gravity wave phase alignment with magnetic meridian as pointed out by *Tsunoda* [2010]. These considerations suggest that the formation of the S-trace involves an instability process operating on the GW-induced density and polarization electric field structures in the presence of an adequate PRE amplitude as is found in the present study.

[16] A further interesting point to note is that unlike in the case of the S-trace, the LSWS has not been observed, or reported to have been observed, with the latitudinal development sequence characterized by its first appearance over the equator and a delayed occurrence over off equatorial latitudes. In the case of the S-trace such a sequence was shown to be a manifestation of the instability growth to form plasma depletions. In this respect there is a subtle difference between the detailed characterizations of these two ESF precursor signatures. In the results by *Tsunoda et al.* [2011] and *Tulasi Ram et al.* [2012], the LSWS signature in the TEC as observed on C/NOFS passes was present with small amplitudes before the E layer sunset and grew in amplitude toward postsunset hours. The F layer height oscillations due to gravity waves reported by *Abdu et al.* [2009b] also presented similar characteristics, that is, the small amplitudes in the late afternoon and presunset hours that increased to large amplitudes in postsunset hours. Due to the larger value of the field line-integrated F region to the E region Pedersen conductivity ratio, the presunset LSWS seen in the F layer heights and TEC must be caused by the gravity wave-induced polarization electric field that can grow in intensity if the conductivity ratio also increases toward sunset. Such an increase of the conductivity ratio toward sunset is expected to occur based on the well-known fact that the sunset decay of E layer ionization takes place faster than that of the F layer ionization (a detailed calculation of the conductivity ratio is, however, necessary to quantitatively support this expectation). The large increase of the

LSWS in the postsunset hours (as seen in the results just cited above) as a last phase of its progressive growth must be due to the contribution from plasma depletion developing through the R-T instability process. It should be noted that *Tsunoda and White* [1981] had shown that the ESF/plasma bubble irregularities grew from the upwellings or crests of the LSWS. It is therefore logical to expect that the irregularity growth through such process is captured in the sequential S-trace occurrences at the equatorial and low-latitude conjugate sites. The first occurrence of the S-trace over the equator is controlled by the PRE (as seen in Figure 3) as an essential factor in the instability growth. On the other hand, the LSWS amplitude that grows toward sunset due to an increasing integrated (*F* to *E* region) conductivity ratio, further increases in amplitude with the postsunset depletion development caused by the PRE. In this way the PRE does have a role to play in the postsunset growth of the LSWS, namely, favoring the instability process leading to the growth of the ESF and plasma depletion, while it does not play any role in the presunset LSWS. On the other hand, the PRE has a direct role in the S-trace development whose dynamics therefore appear to be a manifestation of the direct role of the PRE in the instability process. This explanation implies that the S-trace represents a phase more evolved than the LSWS in the sequence of the processes leading to the postsunset ESF development.

4. Conclusions

[17] The analysis of the ionogram satellite traces as observed at equatorial and low-latitude magnetic conjugate sites by Digisondes has permitted an improved understanding of the connection among the PRE, the LSWS, and the S-trace as precursors for the postsunset ESF development. Such an improved understanding would not have been possible without the observations from conjugate sites. A 3-D model simulation, using the CII mechanism, has helped clarify the nature of the connection among the precursor factors. The main conclusions from the present study may be stated as follows: (1) During the 66 day COPEX (2002) campaign period in Brazil, satellite traces always preceded ESF occurrence at the equatorial and conjugate sites. (2) The occurrence sequence of the S-trace, marked by the first appearance over the magnetic equator followed by a delayed occurrence over the conjugate sites, is consistent with the process of field-aligned vertical growth of plasma bubble over the equator (driven by the R-T instability mechanism) causing latitudinal extension of the depletion extremities to conjugate latitudes, as demonstrated by a 3-D simulation model based on CII mechanism. (3) The S-trace development is related to the prereversal vertical drift enhancement (PRE), always occurring at or after the peak vertical drift causing a seasonally dependent local time shift in its occurrence in association with such displacement in the PRE development. (4) The delay time in the S-trace occurrence at conjugate sites (with respect to the equator) which is related to the nonlinear vertical growth of the bubbles is dependent on the strength of the field line parallel wind, based on the model simulation and therefore is found to decrease from equinoctial to summer season for the COPEX campaign period. (5) The S-trace, though it is related to the LSWS, appears to represent a more advanced phase than the latter in the sequences of the processes connecting precursor conditions to the ESF development.

References

Abdu, M. A., I. S. Batista, and J. A. Bittencourt (1981), Some characteristics of spread F at the magnetic equatorial station Fortaleza, *J. Geophys. Res.*, *86*, 6836, doi:10.1029/JA086iA08p06836.

Abdu, M. A., R. T. Medeiros, J. A. Sobral, and I. S. Batista (1983), Vertical ionization drift velocities and range type spread F in the evening equatorial ionosphere, *J. Geophys. Res.*, *88*, 399–402.

Abdu, M. A., I. S. Batista, B. W. Reinisch, J. H. A. Sobral, and A. J. Carrasco (2006), Equatorial F region evening vertical drift during southern winter months: A comparison of observational data with IRI descriptions, *Adv. Space Res.*, *37*, 1007–1017, doi:10.1016/j.asr.2005.06.074.

Abdu, M. A., I. S. Batista, B. W. Reinisch, J. R. de Souza, J. H. A. Sobral, T. R. Pedersen, A. F. Medeiros, N. J. Schuch, E. R. de Paula, and K. M. Groves (2009a), Conjugate Point Equatorial Experiment (COPEX) campaign in Brazil: Electrodynamics highlights on spread F development conditions and day-to-day variability, *J. Geophys. Res.*, *114*, A04308, doi:10.1029/2008JA013749.

Abdu, M. A., E. A. Kherani, I. S. Batista, E. R. de Paula, D. C. Fritts, and J. H. A. Sobral (2009b), Gravity wave initiation of equatorial spread F/plasma bubble irregularities based on observational data from the SpreadFEx campaign, *Ann. Geophys.*, *27*, 1–16.

Batista, I. S., M. A. Abdu, A. J. Carrasco, B. W. Reinisch, E. R. de Paula, N. J. Schuch, and F. Bertoni (2008), Equatorial spread F and sporadic E-layer connections during the Brazilian Conjugate Point Equatorial Experiment (COPEX), *J. Atmos. Sol. Terr. Phys.*, *70*, 1133–1143, doi:10.1016/j.jastp.2008.01.007.

Chapagain, N. P., B. G. Fejer, and J. L. Chau (2009), Climatology of postsunset equatorial spread F over Jicamarca, *J. Geophys. Res.*, *114*, A07307, doi:10.1029/2008JA013911.

Eccles, J. V. (2004), Assimilation of global-scale and mesoscale electric fields from low-latitude satellites, *Radio Sci.*, *39*, RS1S09, doi:10.1029/2002RS002810.

Fejer, B. G., L. Scherliess, and E. R. de Paula (1999), Effects of the vertical plasma drift velocity on the generation and evolution of equatorial spread F, *J. Geophys. Res.*, *104*, 19,859–19,870, doi:10.1029/1999JA900271.

Fritts, D. C., et al. (2008), Gravity wave and tidal influences on equatorial spread F based on observations during the spread F experiment (SpreadFEx), *Ann. Geophys.*, *26*, 3235–3252.

Kherani, E. A., M. Mascarenhas, J. H. A. Sobral, E. R. de Paula, and F. C. Bertoni (2005), A three dimension simulation model of collisional interchange instability, *Space Sci. Rev.*, *121*, 253–269.

Kherani, E. A., M. A. Abdu, E. R. de Paula, D. C. Fritts, J. H. A. Sobral, and F. C. de Meneses Jr. (2009), The impact of gravity waves rising from convection in the lower atmosphere on the generation and nonlinear evolution of equatorial bubble, *Ann. Geophys.*, *27*, 1657–1668.

Li, G., B. Ning, M. A. Abdu, X. Wan, and L. Hu (2012), Precursor signatures and evolution of post-sunset equatorial spread-F observed over Sanya, *J. Geophys. Res.*, *117*, A08321, doi:10.1029/2012JA017820.

Liu, H.-L., and S. L. Vadas (2013), Large-scale ionospheric disturbances due to the dissipation of convectively generated gravity waves over Brazil, *J. Geophys. Res. Space Physics*, *118*, 2419–2427, doi:10.1002/jgra.50244.

Lyon, A. J., N. J. Skinner, and R. W. Wright (1961), Equatorial spread F at Ibadan, Nigeria, *J. Atmos. Terr. Phys.*, *21*, 100, doi:10.1016/0021-9169(61)90104-0.

Maruyama, T. (1988), A diagnostic model for equatorial spread F: 1. Model description and application to electric fields and neutral wind effects, *J. Geophys. Res.*, *93*, 14,611–14,622, doi:10.1029/JA093iA12p14611.

McClure, J. P., S. Singh, D. K. Bamgboye, F. S. Johnson, and H. Kil (1998), Occurrence of equatorial F region irregularities: Evidence for tropospheric seeding, *J. Geophys. Res.*, *103*, 29,119–29,135.

Reinisch, B. W. (1996), Modern ionosondes, in *Modern Ionospheric Science*, edited by H. Kohl, R. Ruster, and K. Schlegel, European Geophysical Society, pp. 440–458, 37191 Katlenburg-Lindau, Germany.

Reinisch, B. W., M. Abdu, I. Batista, G. S. Sales, G. Khmyrov, T. A. Bullett, J. Chau, and V. Rios (2004), Multistation digisonde observations of equatorial spread F in South America, *Ann. Geophys.*, *22*, 3145–3153, doi:10.5194/angeo-22-3145-2004.

Reinisch, B. W., et al. (2009), The New Digisonde for research and monitoring applications, *Radio Sci.*, *44*, RS0A24, doi:10.1029/2008RS004115.

Röttger, J. (1973), Wave-like structures of large-scale equatorial spread-F irregularities, *J. Atmos. Terr. Phys.*, *35*, 1195–1206, doi:10.1016/0021-9169(73)90016-0.

Thampi, S. V., M. Yamamoto, R. T. Tsunoda, Y. Otsuka, T. Tsugawa, J. Uemoto, and M. Ishii (2009), First observations of large-scale wave structure and equatorial spread F using CERTO radio beacon on the C/NOFS satellite, *Geophys. Res. Letts.*, *36*, L18111, doi:10.1029/2009GL039887.

Tsunoda, R. T. (2008), Satellite traces: An ionogram signature for large-scale wave structure and a precursor for equatorial spread F, *Geophys. Res. Lett.*, *35*, L20110, doi:10.1029/2008GL035706.

Tsunoda, R. T. (2010), On equatorial spread F: Establishing a seeding hypothesis, *J. Geophys. Res.*, *115*, A12303, doi:10.1029/2010JA015564.

Tsunoda, R. T., and B. R. White (1981), On the generation and growth of equatorial backscatter plumes: 1. Wave structure in the bottomside F layer, *J. Geophys. Res.*, *86*, 3610–3616, doi:10.1029/JA086iA05p03610.

Tsunoda, R. T., M. Yamamoto, T. Tsugawa, T. L. Hoang, S. Tulasi Ram, S. V. Thampi, H. D. Chau, and T. Nagatsuma (2011), On seeding, large-scale wave structure, equatorial spread F, and scintillations over Vietnam, *Geophys. Res. Lett.*, *38*, L20102, doi:10.1029/2011GL049173.

Tulasi Ram, S., M. Yamamoto, R. T. Tsunoda, S. V. Thampi, and S. Gurubaran (2012), On the application of differential phase measurements to study the zonal large scale wave structure (LSWS) in the ionospheric electron content, *Radio Sci.*, *47*, RS2001, doi:10.1029/2011RS004870.